Research Square

Preprints are preliminary reports that have not undergone peer review.
They should not be considered conclusive, used to inform clinical practice,
or referenced by the media as validated information.

Monitoring capability of the Dense Seismic Network in Southern Sichuan, China

Yangyang Yu

yuyy219@163.com

Sichuan Seistech Corporation LTD

Xiang Ruan

Sichuan Seistech Corporation LTD

Yuping Shao

Sichuan Seistech Corporation LTD

Yuanxu Zhuang

Sichuan Earthquake Agency

Yu Zhao

Sichuan Earthquake Agency

Research Article

Keywords: Seismic network, Monitoring capability, Location error

Posted Date: November 16th, 2026

DOI: https://doi.org/10.21203/rs.3.rs-10797964/v1

License: This work is licensed under a Creative Commons Attribution 4.0 International License.
Read Full License

Additional Declarations: No competing interests reported.

Monitoring capability of the Dense Seismic Network in Southern Sichuan, China

Yangyang Yu[1*], Xiang Ruan [1], Yuping Shao[1], Yuanxu Zhuang[2], and Yu Zhao[2]

[1]Sichuan Seistech Corporation LTD., Chengdu 610041, China.

[2]Sichuan Earthquake Agency, Chengdu 610041, China.

[*]Corresponding Author: yuyy219@163.com

Abstract: Southern Sichuan is a high-seismic-risk tectonic zone in southwest China, where industrial expansion urgently demands robust microseismic monitoring capacity to mitigate geological hazards. To fill the gap of insufficient detection of small earthquakes due to sparse legacy seismic stations, this study deploys 40 mobile short-period seismic sensors to establish a densely distributed seismic array covering key industrial construction areas. Aiming for a systematic quantification of the network's comprehensive monitoring performance, we develop an integrated evaluation framework that combines two core seismic network metrics: minimum detectable magnitude and hypocenter localization precision. First, based on the spatial layout of stations and measured ambient seismic noise at each observation site, we calculate the theoretical magnitude detection threshold across the entire study area. Second, we apply D-value optimal experimental design theory to quantitatively estimate spatial uncertainties in epicenter and focal depth localization under various source conditions. Third, we propose a multi-factor comprehensive assessment workflow to disentangle the independent and combined effects of focal depth, event magnitude, and the number of synchronous recording stations on overall network monitoring performance. Numerical simulation results confirm that the proposed integrated evaluation method enables rapid, quantitative performance diagnostics for newly deployed dense seismic networks lacking long-term accumulated earthquake catalogs. The resulting spatial distribution maps of detection thresholds and location errors provide actionable quantitative references for subsequent station layout optimization, induced seismicity surveillance, and regional seismic hazard assessment across southern Sichuan and similar fault-active mountainous industrial zones.

Keywords: Seismic network, Monitoring capability, Location error

1. Introduction

1.1 Geological and Engineering Background of the Study Region

The research area is located in southern Sichuan, a region characterized by intense crustal tectonic activity, densely distributed active fault systems, and significant seismic hazard potential [1,2]. Historical earthquake catalog statistics indicate that nearly all natural and anthropogenically induced microseismic in this region originate at focal depths between 1 km and 10 km below the surface [2,3]. Prior to the deployment of the dense mobile seismic network described herein, the permanent regional seismic observation network had very sparse station spacing, resulting in two major limitations: a limited ability to detect microseismic events below magnitude 1.0, and considerable spatial bias in hypocenter location accuracy.

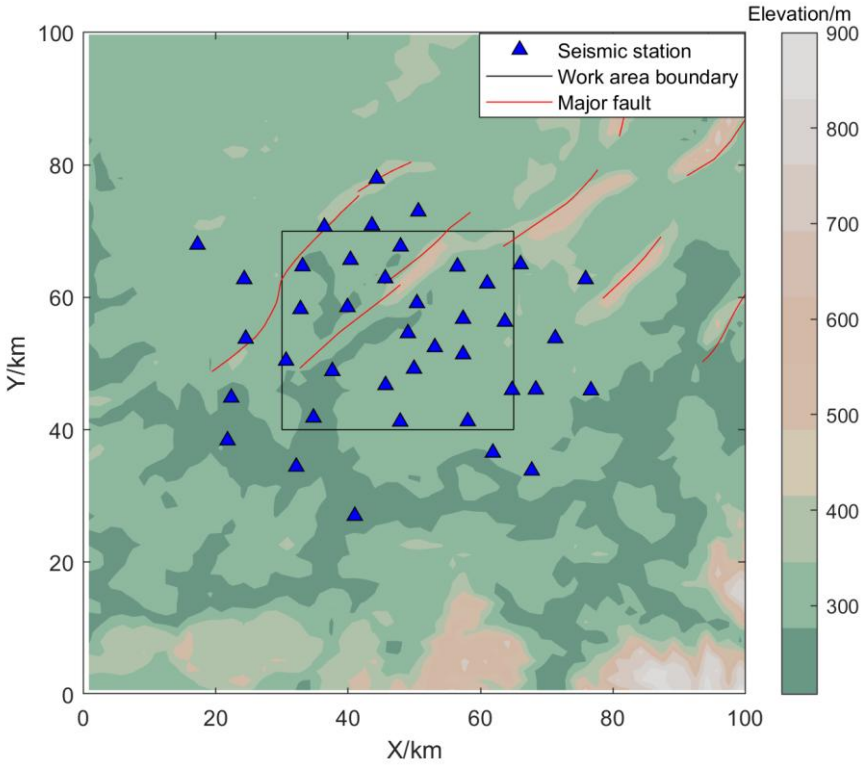


Figure 1. Stations distribution of the dense seismic network in Southern Sichuan

Driven by large-scale industrial development, underground fluid extraction, and associated production safety requirements, 40 portable short-period seismic stations were deployed throughout the study area to build a high-density seismic monitoring network. The inter-station

distances are maintained between 5 km and 10 km, creating a closed observation coverage over the core engineering zones (Figure 1). This custom-built engineering seismic array is designed to continuously monitor local microseismic activity while providing standardized waveform and hypocenter datasets to support fault activity characterization, seismic risk zoning, and emergency hazard response [4].

1.2 Research Progress on Seismic Network Performance Evaluation

Seismic monitoring networks constitute the essential observational infrastructure for multidisciplinary geoscience research, encompassing seismicity statistics, aftershock tracking, crustal velocity tomography, and analysis of induced seismicity mechanisms. The overall monitoring capacity of a seismic array serves as a key quantitative indicator for assessing the reliability of its observational data [5,6]. Rigorous, quantitative evaluation of network performance holds significant practical value for earthquake monitoring, seismic prediction, and deep structural geophysical exploration [7,8]. In this context, developing a unified assessment system for newly constructed dense seismic arrays has become an urgent technical necessity.

Existing evaluation methodologies for seismic network monitoring capacity can be categorized into two mutually independent branches: the assessment of the minimum complete detectable magnitude and the quantification of hypocenter localization accuracy [9].

For the evaluation of minimum detectable magnitude, mainstream statistical seismology approaches rely entirely on historical earthquake catalogs. Representative algorithms include the maximum curvature (MAXC) method, the goodness-of-fit (GFT) fitting algorithm [10], full magnitude range (EMR) completeness analysis [11], repeated-earthquake spatial capacity inversion [12], and probability-based magnitude of completeness (PMC) modeling [13,14]. All these catalog-dependent techniques require years of accumulated seismic event records, making them unsuitable for pre-operation or real-time performance assessment of newly established stations. Alternatively, theoretical forward-calculation schemes estimate detection thresholds using seismic magnitude attenuation relations and site ambient noise measurements [15]. However, these purely synthetic calculations overlook real ground motion transmission heterogeneities,

resulting in systematic discrepancies between theoretical predictions and actual field monitoring performance.

In the field of hypocenter localization capacity evaluation, Sato et al. pioneered the use of Monte Carlo stochastic simulations to analyze positioning uncertainty for seismic arrays [16]. Subsequently, Kijko developed the D-value optimal design theory tailored to microseismic network layout optimization. This theory reflects the overall positioning stability of a station group but does not provide detailed spatial error distribution [17]. Gong et al. expanded the D-value theory into a comprehensive network optimization and evaluation platform, enabling pixel-level quantitative calculations of theoretical hypocenter errors [18]. Complementary calibration methods employ controlled blasting events to verify the real-world location precision of operational seismic networks [19]. More recently, Gao et al. incorporated weighted objective functions into D-optimal design to enhance microseismic station deployment schemes [20].

1.3 Existing Limitations of Current Evaluations and Research Design of This Work

A significant limitation of current research is the widespread use of single-indicator evaluation frameworks. Most published studies either independently calculate the network's minimum detectable magnitude or separately quantify spatial positioning errors, with very few integrated workflows that combine both core metrics to provide a systematic and comprehensive characterization of overall monitoring capacity [21,22]. Isolated single-index analyses can only partially reflect array performance and cannot disentangle the combined effects of signal detectability and positioning precision under complex topographic, geological, and station layout conditions.

For the dense mobile array examined in this paper, the limited operation time and the insufficient number of spatially uniform recorded microseismic events hinder reliable catalog-based statistical evaluation. To overcome this limitation, the present study employs a noise-based theoretical forward model to calculate spatial magnitude detection thresholds, combined with regionally calibrated D-value optimal design theory to map epicenter and depth error distributions throughout the entire domain. By integrating magnitude detection performance

and localization uncertainty into a unified evaluation framework, we establish a comprehensive workflow for assessing network capacity.

Building on multi-objective regional seismic network evaluation frameworks proposed in recent literature [23,24], this study further refines the integrated assessment pipeline by incorporating three key controllable variables: regional earthquake focal depth distribution, local magnitude detection thresholds, and the minimum number of synchronous effective observation stations required for stable three-dimensional hypocenter inversion. Compared to fully Bayesian optimal experimental design, which incurs prohibitive computational costs for full-grid regional simulation [25], the D-value theory employed here strikes a balance between high computational efficiency and robust quantification of positioning uncertainty. This makes it particularly well-suited for performance evaluation of large-area, dense mobile arrays deployed in mountainous industrial zones [20].

From an application perspective, this paper complements targeted case research on short-period dense mobile seismic networks within high-seismic-risk zones of southwest China. Most relevant international literature focuses on small-aperture nodal dense arrays or permanent regional fixed-station networks [20, 26, 27], while domestic evaluation cases predominantly involve long-term provincial fixed seismic observation stations [7, 12]. The integrated magnitude–location error evaluation framework developed in this research provides quantitative layout optimization guidelines for similar monitoring networks deployed for fluid extraction, underground energy storage, and fault surveillance across southern Sichuan and adjacent tectonically active regions.

2. Methods

This study proposes a three-stage rapid quantitative evaluation workflow for assessing the monitoring capacity of dense seismic networks: (1) Forward calculation of the theoretical spatial distribution of the minimum detectable magnitude, constrained by station ambient noise and seismic signal attenuation models; (2) Quantitative estimation of spatial epicenter and focal depth localization errors using D-value optimal design theory; (3) Comprehensive multi-condition

evaluation that decouples and quantifies the effects of focal depth, event magnitude, and the number of effective recording stations on overall monitoring performance.

2.1 Evaluation of Theoretical Magnitude Monitoring Capability

The magnitude monitoring capability of a seismic network is illustrated through spatial contour maps depicting the minimum detectable local magnitude M_L. This detection threshold is determined by a combination of station spatial density, geometric configuration, and ambient background noise levels at each sensor site.

For the 40-station array used in this study, station coordinates and inter-site spacing (5–10 km) were fixed following field deployment. To obtain stable and representative background noise measurements at each station, we extracted 24-hour continuous seismic waveform segments free from identifiable seismic signals and intense anthropogenic vibration interference. The raw waveform data underwent dual quality control: visual inspection of time-series traces and spectrogram frequency-domain screening to eliminate transient seismic signals. Standard preprocessing procedures were then applied, including instrument response deconvolution, linear trend removal, and band-pass filtering tailored to the sensor's effective frequency band. Averaging the full-day filtered waveforms produced stable root-mean-square ambient noise velocity values V_n for each observation point.

This study focuses on shallow local microseismic within the study area, using the absolute maximum horizontal-component S-wave amplitude V_s as the primary observable for calculating local magnitude. A signal-to-noise ratio (SNR) threshold of ≥6 is applied to ensure reliable seismic phase picking and clear signal identification at recording stations, $V_s \geq 6 \times V_n$.

In compliance with China's national standard GB17740-2017, "Regulation of Earthquake Magnitude Determination" [28], the near-source body-wave magnitude formula for digital seismic networks is implemented:

$$M_L = \lg(V_s) + R(\Delta) \quad (1)$$

Where M_L is the local magnitude, V_s is the absolute maximum S-wave horizontal

amplitude recorded, and $R(\Delta)$ is the distance correction term. Δ is the distance from the source to the station. We use R_{13} from GB17740-2017, which is calibrated for the Sichuan region [28].

Earthquake location inherently limits the number of available recording stations: planar epicenter localization requires a minimum of three stations, while stable 3D location (simultaneously determining epicenter coordinates and focal depth) requires at least four synchronous station records [29]. Engineering seismology practice further confirms that reliable estimation of complete seismic source parameters and quantitative location error bounds necessitates no fewer than four valid observation stations [30,31]. Therefore, we define the effective monitoring domain as the geographic region where any virtual seismic source can generate identifiable signals recorded by four or more stations that meet the SNR≥6 criterion.

We use the earthquake sequencing method to calculate the spatial distribution of the minimum detectable magnitude. The entire study area is divided into uniform grid cells measuring 1 km × 1 km, with each grid node considered a potential virtual source. For each virtual source, we compute the theoretical magnitude detectable at each station, sort these magnitudes from smallest to largest, and select the fourth smallest magnitude as the minimum detectable magnitude for that source. This calculation is repeated for all grid nodes, and contour maps are generated to illustrate the spatial distribution of magnitude monitoring capability [32,33].

2.2 Earthquake Location Error Calculation Based on D-Value Optimal Design Theory

Proposed by Kijko, the D-value optimal design theory was originally developed to optimize the geometric layout of microseismic monitoring networks. Its core principle focuses on minimizing the determinant of the hypocenter parameter covariance matrix [17]. A smaller determinant of the covariance matrix indicates tighter confidence intervals for the parameters and higher overall precision in earthquake localization.

Define the source parameter vector is $H(x_0, y_0, z_0, t_0)$, the station coordinate is $X_i(x_i, y_i, z_i)$ and numbered is $i(i = 1,2,3,...,n)$, v_p is the velocity of P-wave in the medium, t_0 is the origin time of the earthquake, t_i is the time of the station *i* receives the signal of P-wave, the travel time from the source *H* to the station *i* is:

$$T_i(H, v_0, X_i) = t_i - t_0 = \frac{\sqrt{(x_i - x_0)^2 + (y_i - y_0)^2 + (z_i - z_0)^2}}{v_p} \quad (2)$$

The partial derivative matrix of relative travel time of source parameters is:

$$A = \begin{Bmatrix} 1 & \frac{\partial T_1}{\partial x_0} & \frac{\partial T_1}{\partial y_0} & \frac{\partial T_1}{\partial z_0} \\ \vdots & \vdots & \vdots & \vdots \\ 1 & \frac{\partial T_n}{\partial x_0} & \frac{\partial T_n}{\partial y_0} & \frac{\partial T_n}{\partial z_0} \end{Bmatrix} \quad (3)$$

Considering the random errors of the P-wave velocity σv_p, and the pickup error of arrival time of P-wave σt_p. A diagonal matrix W is established, which is the random error matrix, and the diagonal elements are:

$$W = \frac{1}{(\frac{\partial T_i}{\partial v_p})^2 (\sigma v_p)^2 + (\sigma t_p)^2} \quad (4)$$

Covariance matrix is:

$$C = (A^T W A)^{-1} \quad (5)$$

Kijko defined the standard deviation of the epicenter position as the radius of a plane [12], thus determining the epicenter positioning error as:

$$\mathrm{d}h = \sqrt{\sqrt{C_{22} C_{33} - C_{23}^2}} \quad (6)$$

And the depth error of the source is:

$$\mathrm{dz} = \sqrt{C_{44}} \quad (7)$$

Where C_{22}, C_{33}, and C_{44} are the diagonal elements of the covariance matrix C, and C_{23} is the element in row 2, column 3 of matrix C.

For this study, a regionally calibrated one-dimensional velocity model of the Sichuan crust is adopted [34,35], v_p=6000 m/s at 10 km depth and v_p=5000 m/s at 5 km depth. The v_p / v_s ratio is approximately 1.73, consistent with the regional crustal structure. The P-wave velocity error is set to 1%, and the arrival-time picking error is 0.01 s, corresponding to a sampling rate of 100 Hz is the natural frequency of the seismic data.

2.3 Integrated Comprehensive Evaluation Framework

The integrated assessment workflow combines magnitude detection capability and hypocenter localization error to quantify overall network monitoring performance. The independent calculations in Sections 2.1 and 2.2 assume that all stations within range successfully detect seismic signals; however, in real observation scenarios, the number of valid recording stations varies significantly depending on earthquake magnitude and spatial position. To account for this physical constraint, we impose a minimum threshold of four valid recording stations, which is required for stable 3D hypocenter inversion, and then compute theoretical monitoring performance for discrete combinations of earthquake magnitude and focal depth.

Consistent with regional seismicity statistics indicating dominant focal depths of 1–10 km [1], two representative depth planes (5 km and 10 km) were selected to isolate depth-dependent variations in array detection and positioning capabilities. By comparing simulation outputs between these two depth horizons, we systematically analyze how source burial depth influences the network's overall monitoring performance.

3. Application to the Dense Mobile Seismic Network in Southern Sichuan

The dense seismic array deployed for this research consists of 40 GL-CS2 three-component short-period seismometers paired with EDAS-24GN 24-bit high-resolution data loggers, all operating at a uniform sampling rate of 100 Hz. Each sensor provides a flat amplitude frequency response across the 2 Hz to 50 Hz band, optimized for seismic event recording. Field deployment was completed in 2026, and the network has maintained uninterrupted continuous operation to date. Complete station metadata, including horizontal coordinates, surface elevation, and measured ambient noise velocity (V_n, μm/s), are summarized in Table 1.

Table 1. Geometric Parameters and Ambient Background Noise Velocity for All 40 Seismic Stations

Station NO.	X (km)	Y (km)	Z (m)	Vn (μm/s)	Station NO.	X (km)	Y (km)	Z (m)	Vn (μm/s)
T01	54.94	54.13	348	0.067	T21	50.16	69.16	292	0.114
T02	67.11	68.30	377	0.750	T22	44.38	72.21	309	0.049
T03	38.24	46.01	255	0.034	T23	48.74	85.72	300	0.015
T04	36.42	71.15	290	0.084	T24	45.10	29.70	300	0.062
T05	52.71	74.44	313	0.098	T25	70.04	61.94	389	0.046

T06	33.68	55.46	311	0.053	T26	41.37	53.75	303	0.076
T07	24.57	49.33	282	0.170	T27	62.16	71.12	351	0.053
T08	26.98	59.11	317	0.065	T28	75.18	50.68	352	0.057
T09	53.93	60.04	313	0.039	T29	35.38	37.86	294	0.050
T10	58.40	57.72	331	0.170	T30	23.96	42.23	305	0.053
T11	63.10	56.53	366	0.016	T31	50.22	51.41	342	0.049
T12	63.10	62.42	337	0.071	T32	52.65	45.33	295	0.051
T13	55.43	65.03	297	0.035	T33	68.05	40.18	298	0.046
T14	26.73	69.01	309	0.036	T34	72.64	71.50	353	0.047
T15	18.96	74.74	315	0.023	T35	83.46	69.01	310	0.063
T16	43.89	64.37	311	0.073	T36	84.34	50.54	345	0.073
T17	47.96	77.95	313	0.030	T37	71.24	50.60	308	0.045
T18	55.66	80.27	306	0.135	T38	63.88	45.41	330	0.036
T19	36.08	64.04	316	0.038	T39	78.42	59.19	397	0.037
T20	40.05	77.71	333	0.039	T40	74.50	37.20	336	0.057

3.1 Spatial Distribution of the Minimum Detectable Magnitude at Two Focal Depths

The study area is discretized into uniform 1 km grid cells for virtual source forward modeling, with separate full-domain magnitude threshold calculations performed for the 10 km and 5 km focal depth horizons.

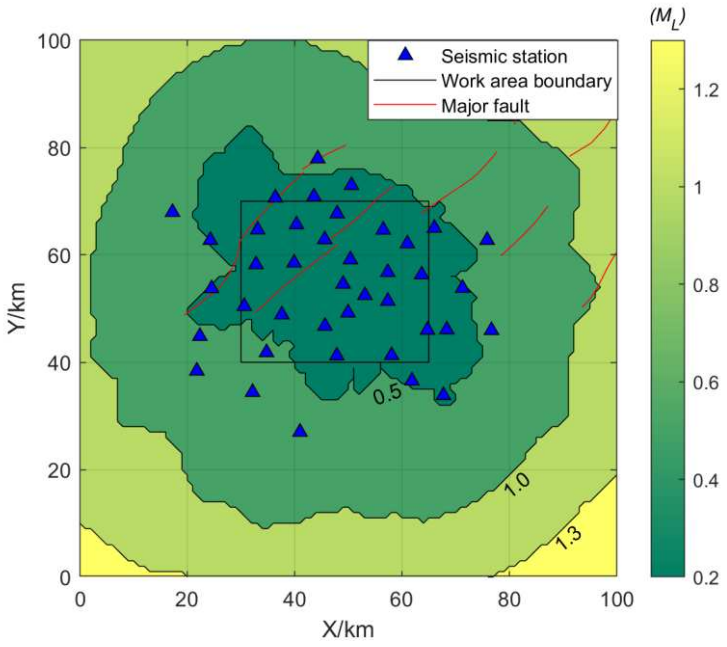


Figure 2. Contour map of the monitoring capability for the theoretical magnitude of the seismic network, with a focal depth of 10 km.

For events originating at a depth of 10 km (Figure 2), approximately 90% of the entire work

area achieves a minimum detectable magnitude of M_L 0.5. The majority of the monitoring domain reliably detects earthquakes of magnitude M_L 1.0, and no geographic region within the array's coverage fails to detect seismic events of magnitude M_L 1.3 or greater.

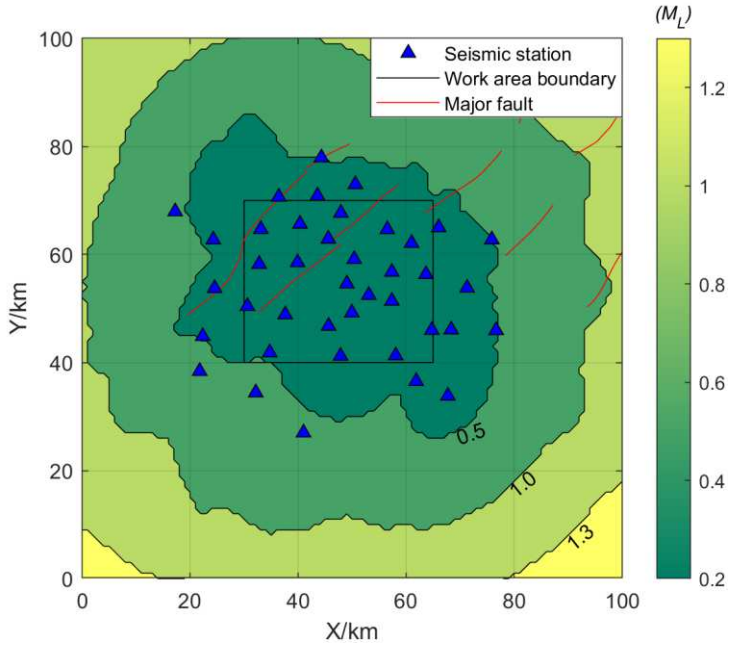


Figure 3. Contour map of the monitoring capability for the theoretical magnitude of the seismic network, with a focal depth of 5 km.

At the shallower focal depth of 5 km (Figure 3), coverage of the M_L 0.5 detection threshold expands to 100% of the work domain. The spatial extent of regions capable of resolving M_L 1.0 and M_L 1.3 events shows negligible variation compared to the 10 km depth case. This comparison confirms that shallower seismic sources significantly enhance the network's ability to detect small seismic events below M_L 0.8, while detection performance for moderate earthquakes ($M_L \geq 1.0$) remains nearly unchanged with focal depth variations within the 1–10 km range.

3.2 Theoretical Earthquake Location Errors at Focal Depths of 5 km and 10 km

D-value optimal design theory is applied to generate full-domain spatial contour maps of horizontal epicenter error and vertical focal depth error for source depths of both 10 km and 5 km. All simulations assume seismic events with sufficient amplitude to produce SNR of 6 or greater at all nearby stations.

The focal depth is set at 10 km (Figure 4a, 4b). Horizontal epicenter positioning errors range from 20 m to 100 m across the domain. Within the densely instrumented core working zone,

horizontal errors are consistently reduced to less than 20 m. Vertical focal depth errors vary from 50 m to 300 m; however, core station clusters achieve depth precision better than 50 m, and nearly all regions within the network's outer boundary maintain depth errors below 100 m.

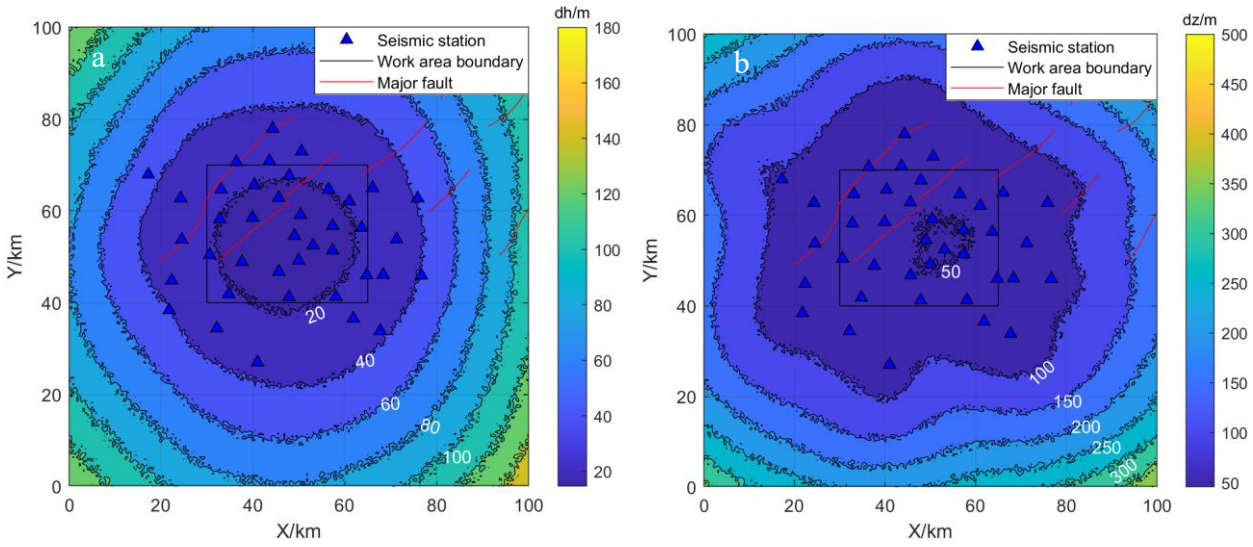


Figure 4. Contour map of the theoretical epicenter positioning error (a) and depth positioning error (b) of the seismic network, with a focal depth of 10 km.

The focal depth is set at 5 km (Figure 5a, 5b). Horizontal epicenter positioning precision improves slightly compared to the 10 km depth case, with the entire work area exhibiting epicenter errors smaller than 20 meters. Vertical depth errors display varying spatial trends: densely covered central zones experience slight reductions in depth uncertainty, while peripheral areas distant from station clusters show increased depth errors, with maximum vertical errors reaching up to 400 meters at the network's outermost edges.

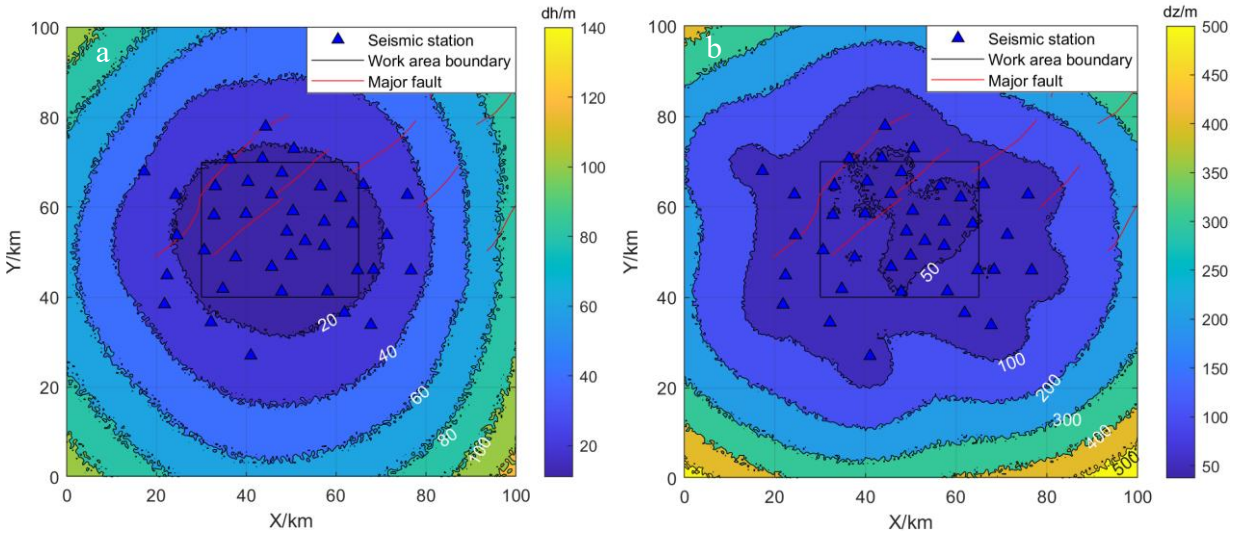


Figure 5. Contour map of the theoretical epicenter positioning error (a) and depth positioning error (b) of the seismic network, with a focal depth of 5 km.

Synthesizing both depth planes reveals two universal patterns: horizontal epicenter localization errors are consistently smaller than vertical focal depth errors under identical source conditions, and station density serves as the dominant controlling variable—higher local station density directly correlates with reduced spatial positioning uncertainty in both horizontal and vertical dimensions.

3.3 Relationship Between Location Error and Event Magnitude

The preceding location error simulations assume that all surrounding stations successfully record seismic signals, which is only valid for relatively large-magnitude events. For small earthquakes, only stations within a limited epicenter distance meet the SNR ≥ 6 detection criterion; having fewer valid recording stations directly reduces the stability of hypocenter inversion and increases positioning errors. This subsection separates simulations by event magnitude at fixed focal depths to quantify the magnitude-dependent localization precision.

The focal depth is set at 10 km, for M_L 0.5 earthquake magnitude (Figures 6a and 6b). Only the central part of the array achieves an epicenter error of less than 100 meters and a depth error below 300 meters. The outer areas lack four valid recording stations, making stable 3D earthquake location impossible in those regions.

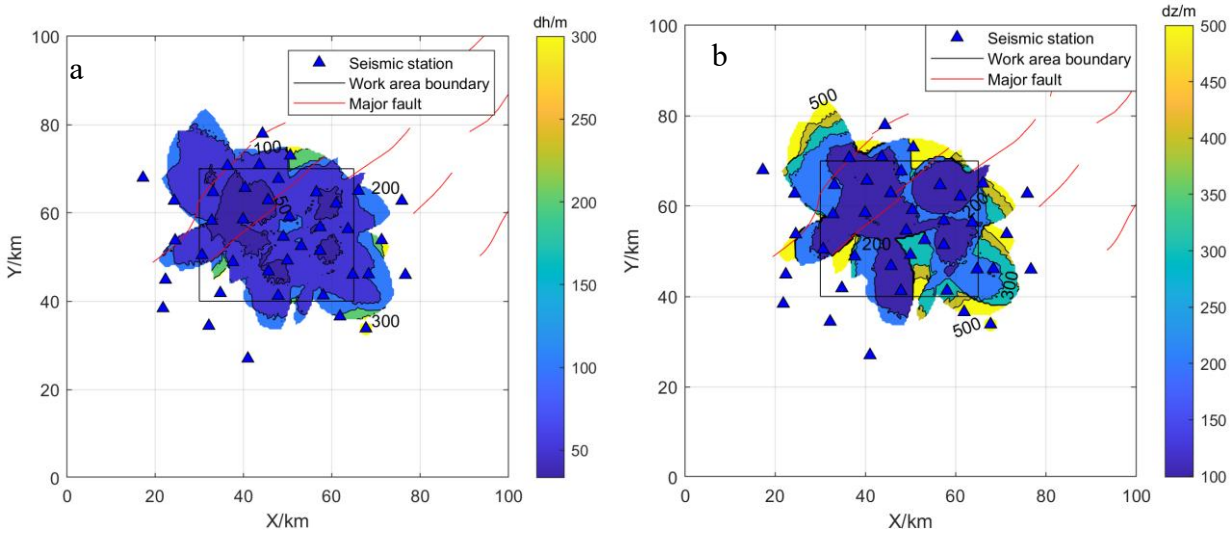


Figure 6. Contour map of the theoretical epicenter positioning error (a) and depth positioning error (b) of the

seismic network, with a focal depth of 10 km, and for M_L 0.5 earthquake magnitude.

The focal depth is set at 10 km, for M_L 1.0 earthquake magnitude (Figures 7a and 7b). Valid signal coverage extends to nearly the entire study area. Horizontal epicenter error decreases to less than 40 meters across work regions, while vertical depth error remains within 100 meters in the core monitoring zone.

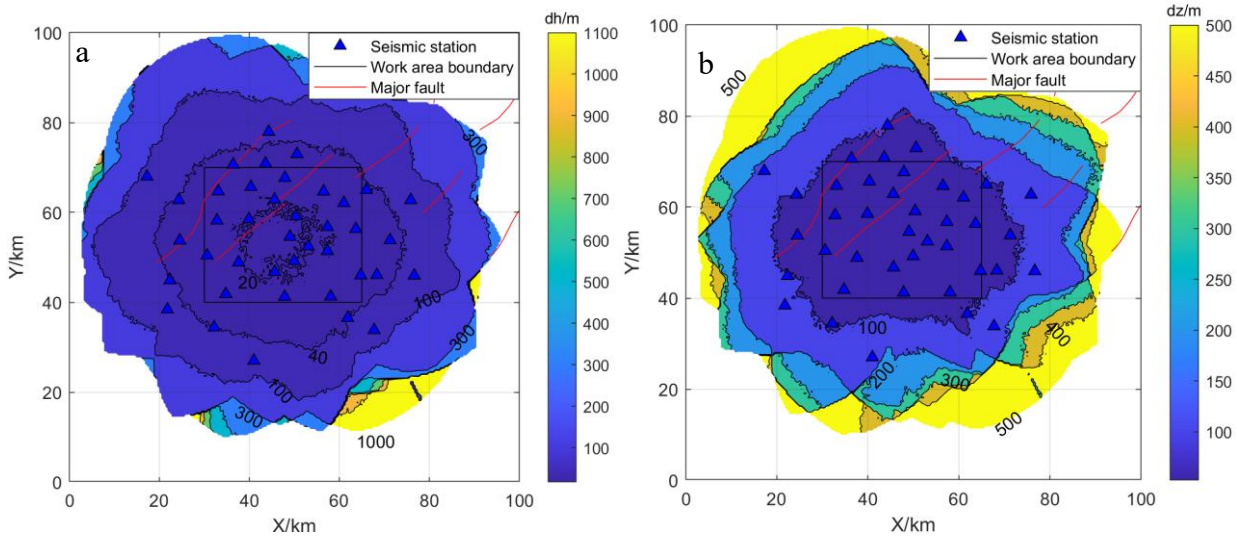


Figure 7. Contour map of the theoretical epicenter positioning error (a) and depth positioning error (b) of the seismic network, with a focal depth of 10 km, and for M_L 1.0 earthquake magnitude.

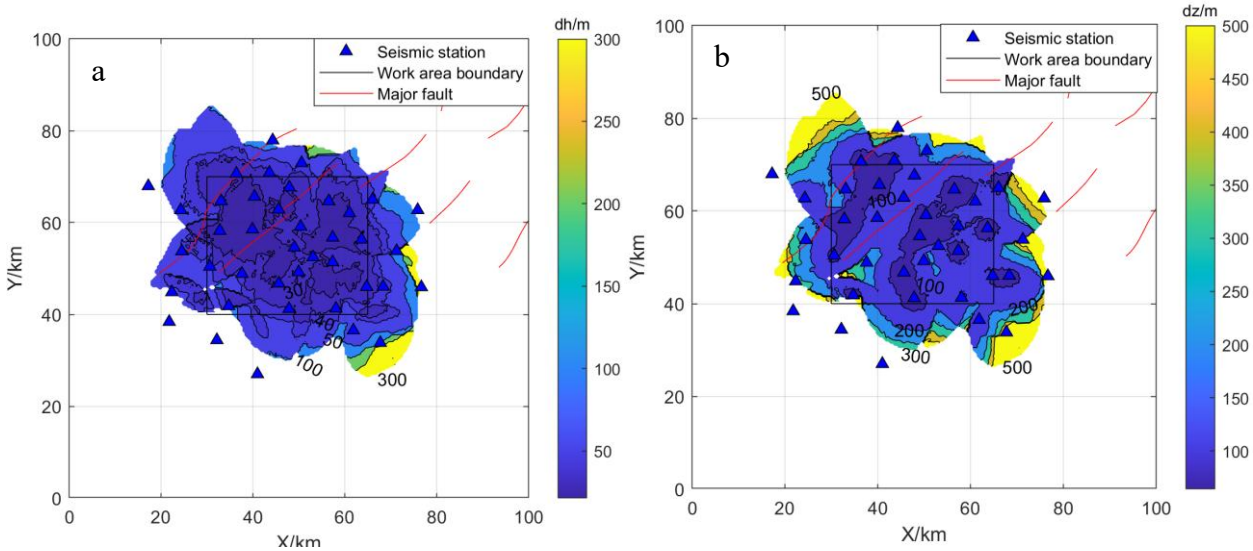


Figure 8. Contour map of the theoretical epicenter positioning error (a) and depth positioning error (b) of the seismic network, with a focal depth of 5 km, and for M_L 0.5 earthquake magnitude.

The focal depth is set at 5 km, for M_L 0.5 earthquake magnitude (Figures 8a and 8b). Shallow M_L 0.5 sources produce detectable signals across a wider area than events of the same

magnitude located at a depth of 10 km. Within the reliable detection zone, the errors in epicenter location are less than 50 meters, and the errors in vertical depth are below 200 meters, indicating a noticeable increase in accuracy compared to deeper and low-magnitude earthquakes.

Overall, the simulation results reveal two main patterns: higher magnitude events trigger more synchronized recording stations, which broadens effective monitoring coverage and decreases uncertainty in both horizontal and vertical positioning. Additionally, shallower focal depths increase the seismic signal strength at surface stations, resulting in a greater number of valid observation points and enhancing localization accuracy at a given magnitude.

3.4 Discussion

This study provides a completely theoretical quantitative evaluation of the newly installed dense mobile seismic array in southern Sichuan. The distinctly spatial pattern of earthquake location errors (as shown in Figures 6 and 8) primarily results from the irregular geometric arrangement of earthquake stations, with additional contributions from regional subsurface geological variations and spatial differences in seismic wave attenuation.

The assessment focuses on earthquakes with magnitudes less than 1.5. These events provide essential data for understanding the evolution of microseismic activity, mapping detailed active fault structures, and conducting quantitative seismic hazard assessments.

The integrated evaluation approach presented here provides clear advantages for newly established seismic networks that lack long-term continuous earthquake records. Compared to older, sparse regional seismic stations, the dense mobile array reduces the minimum detectable earthquake magnitude to ML0.5 and improves earthquake location accuracy within the primary industrial monitoring area

Two primary limitations affect this study: the use of a simplified one-dimensional layered crustal velocity model and the assumption of uniform seismic wave attenuation across the study area, which neglects small-scale lateral geological variations. Future research will incorporate three-dimensional tomographic crustal velocity models calibrated with local explosion and earthquake data, along with accumulated real seismic waveforms from the dense array, to reduce systematic errors and improve the accuracy of network performance predictions.

4. Conclusions

This research develops a unified theoretical evaluation system for dense seismic monitoring networks by integrating minimum magnitude detection capacity calculations with D-value theory-based hypocenter location error quantification. The target array comprises 40 portable short-period seismic stations deployed in 2026 across southern Sichuan, with controlled inter-station spacing of 5–10 km. The key research conclusions are summarized as follows:

1. Magnitude Detection Performance: The network reliably identifies earthquakes as small as M_L 0.5 across 90%–100% of the work area. Shallow focal depths (5 km) provide superior ultra-microseismic detection capabilities compared to deeper sources at 10 km.

2. Hypocenter Localization Precision: The horizontal epicenter positioning error remains below 100 meters across nearly all work regions, while the vertical focal depth error predominantly stays under 300 meters. Localization accuracy improves consistently with increasing event magnitude and decreasing source burial depth, due to a greater number of synchronous valid recording stations.

3. Engineering Application Value: The integrated multi-factor evaluation workflow enables rapid, fully quantitative performance diagnostics for newly established dense seismic arrays that lack sufficient accumulated seismic event records. The resulting spatial contour maps offer direct quantitative support for iterative station layout optimization, induced seismicity monitoring, and enhanced seismic hazard assessment in high-risk tectonic zones.

The theoretical assessment methodology developed in this paper provides actionable technical guidance for post-deployment station densification, layout readjustment, and overall performance optimization of seismic monitoring networks distributed across fault-active, high-seismic-risk regions in southwest China.

Data Availability Statement:

All data generated or analysed during this study are included in this published article. The original seismic waveform data are available from the corresponding author on reasonable request.

Declarations:

Competing interests

The authors declare no competing interests.

Ethical approval

This study did not involve human participants or animals, and therefore ethical approval was not required.

Consent to participate

Informed consent was not required as no human participants were involved in the study.

Consent to publish

This manuscript does not contain any individual person's data in any form.

Credit Author Statement：

Yangyang Yu, Xiang Ruan, Yuping Shao, Yuanxu Zhuang, and Yu Zhao, wrote the main manuscript text and prepared figures 1-8. All authors reviewed the manuscript.

Author Contributions:

Yangyang Yu: Conceptualization; Supervision; Writing – original draft.

Xiang Ruan: Resources; Review & Editing; Visualization.

Yuping Shao: Resources; Data curation.

Yuanxu Zhuang: Writing – review & editing; Visualization.

Yu Zhao: Supervision; Review & Editing;

Funding declaration： This research was funded by the Young Scientists Fund of the National

Natural Science Foundation of China, grant number 42104058.

References

1. Lei, X.L.; Wang, Z.W.; Su, J.R. The December 2018 ML 5.7 and January 2019 ML 5.3 Earthquakes in South Sichuan Basin Induced by Shale Gas Hydraulic Fracturing. *Seismol. Res. Lett.* **2019**, 90, 1099–1110. DOI:10.1785/02190096.
2. Yi G. X.; Long F.; Liang M. J.; et al. Focal mechanism solutions and seismogenic structure of the June 17, 2019 Ms6.0 Changning earthquake, Sichuan. *Chinese Journal of Geophysics*, **2019**, 62:3432-3447. DOI: 10.6038/cjg2019N0297.
3. Zhang Z. W.; Long F.; Wang S. Y. Earthquake location and velocity structure in Yibin area, Sichuan. *Seismology and Geology*, **2019**, 41:913-926.
4. Qi G. L.; Yuan C.; Yu M.; Tang L. Optimization of local seismic network layout based on seismic monitoring capability. *Acta Seismologica Sinica*. **2022**, 44, 476−488. DOI: 10.11939/jass.20210019.
5. Qiu, Y.; Jiang, C. S.; Si, Z. Y. Summary of Technical Methods for Optimizing Layout of Seismic Monitoring Network. *Prog. Geophys.* **2020**, 35, 866–873. DOI:10. 6038/pg2020DD0069
6. Wang, P.; Zheng, J.; Li, B. Monitoring Ability Evaluation of Shandong Seismological Network Based on PMC Method. *Prog. Geophys.* **2016**, 31, 2408–2414.
7. Wang, Y.; Jiang, C.; Liu, F.; Bi, J. Evaluation of Monitoring Ability of China Seismological Network and Station Scoring (2008–2015). *Chin. J. Geophys*. **2017**, 60, 261–272.
8. Liu, F.; Jiang, C.; Zhang, F.; Yang, Y.; Liang, Y.; Wang, L.; Miao, C. Study on Monitoring Capability of Regional Seismic Network in Inner Mongolia. *Acta Seismol. Sin*. **2014**, 36, 919–929.
9. Li, R. Study on Monitoring Ability of Hulunbeier Area Based on Ground Pulsation Noise. *J. Disaster Prev. Mitig. Eng*. **2019**, 35, 60–63.
10. Wiemer, S.; Wyss, M. Minimum Magnitude of Completeness in Earthquake Catalogs: Examples from Alaska, the Western United States, and Japan. *Bull. Seismol. Soc. Am*. **2000**, 90, 859–869. DOI:10.1785/0119990012.
11. Woessner, J.; Wiemer, S. Assessing the Quality of Earthquake Catalogs: Estimating Magnitude of Completeness and Its Uncertainty. *Bull. Seismol. Soc. Am*. **2005**, 95, 684–698. DOI:10.1785/0120040037.
12. Jiang, C.; Wu, Z. Estimation of Positioning Accuracy of China Seismological Network Based on Repeated Earthquakes. *Earthq. Res. China.* **2005**, 21, 147–154.
13. Schorlemmer, D.; Woessner, J. Probability of Detecting an Earthquake. *Bull. Seismol. Soc. Am.* **2008**, 98, 2103–2117. DOI:10.1785/0120070079.

14. Schorlemmer, D.; Mele, F.; Marzocchi, W. Magnitude of Completeness Analysis of the Italian National Seismic Network. *J. Geophys. Res*.**2010**, 115, B04308. DOI:10.1029/2009JB006947.
15. Sereno, T.J.; Bratt, S.R. Seismic Detection Capability at NORESS and Implications for Network Detection Thresholds. *J. Geophys. Res*. **1989**, 94, 10397–10414. DOI:10.1029/JB094iB08p10397.
16. Sato, Y.; Skoko, D. Optimum Distribution of Seismic Observation Points, II. *Bull. Earthq. Res. Inst*. **1965**, 43, 451–457.
17. Kijko, A. An Analysis of the Accuracy of Location of Local Earthquakes Depending on the Number of Seismic Stations. *Pure Appl. Geophys*. **1977**, 115, 1011–1021.
18. Gong, S.; Dou, L.; Cao, A.; He, H.; Du, T.; Jiang, H. Research on Optimal Layout of Microseismic Monitoring Network in Coal Mine. *Chin. J. Geophys*. **2010**, 53, 457–465.
19. Guo, B.; Liu, Q.; Chen, J.; Li, S. Microseismic Location Experiment of Digital Seismic Network in the Capital Region. *Seismol. Geol*. **2002**, 24, 453–460.
20. Gao, Y. T.; Wu, Q. L. Wu S. C.; Ji M. W.; Cheng A. P.; Yang K. Optimization of microseismic monitoring networks based on the theory of D-optimal design. *Chinese Journal of Engineering*. **2013**, 35, 1538-1545. DOI: 10.13374/j.issn1001-053x.2013.12.005
21. Wu, K.; Jiao, Y.; Yang, M. Optimization Scheme of China Seismological Network Layout. *J. Seismol*. **1991**, 1, 22–37.
22. Cai Y. Q,; Yu Z. Y.; Wang W. T.; Liao S. R.; Tang L.; Pang Y.; Yang W. Transfer learning research on seismic phase detection models based on Early Warning Data from Sichuan region. *Acta Seismologica Sinica*. **2025**, 47, 889−908. DOI:10.11939/jass.20240102
23. Fuggi, A.; Re, S.; Tango, G.; Del Gaudio, S.; Brovelli, A.; Cassiani, G. Assessment of Earthquake Location Uncertainties for the Design of Local Seismic Networks. *Earthq. Sci.* **2024**, 37, 415–433. DOI:10.1016/j.eqs.2024.06.006.
24. Huang, X.; Li, S.; Dong, L.; Yang, L. Optimization Research on Sensor Network Layout for Microseismic Monitoring Based on Location Error Analysis. *Sensors.* **2026**, 26, 4533. DOI:10.3390/s26144533.
25. Callahan, J.; Monogue, K.; Villarreal, R.; Catanach, T. Analysis and Optimization of Seismic Monitoring Networks with Bayesian Optimal Experimental Design. *Geophys. J. Int*. **2025**, 240, 1802–1824. DOI:10.1093/gji/ggae458.
26. Savvaidis, A., Young, B., Huang, G., & Lomax, A. TexNet: A statewide seismological network in Texas. *Seismological Research Letters*. **2019**, 4, 1702–1715.
27. Aziz Zanjani, A., DeShon, H. R., Karanam, V., & Savvaidis, A. Insights into spatiotemporal evolution of induced earthquakes in the southern Delaware Basin using calibrated relocations from the TexNet catalog (2017–2022). *Earth and Space Science*. **2025**, 12, e2024EA004027. DOI:10.1029/2024EA004027.
28. GB17740-2017. Regulation of Earthquake Magnitude; China Earthquake Agency: Beijing, China, **2017**.

29. Aki, K.; Richards, P.G. Quantitative Seismology, 2nd ed.; University Science Books: Sausalito, USA, **2002**.
30. Wu, K.; Jiao, Y.; Yang, M. Optimization Scheme of China Seismological Network Layout. *J. Seismol.* **1991**, 1, 22–37.
31. Ji, A.; Shi, Y. Evaluation of Earthquake Monitoring Capability of Shandong Digital Telemetry Seismic Network. *Plateau Earthq.* **2001**, 13, 47–52.
32. Xie, J.; Liu, S.; Sun, L. MATLAB Implementation of Regional Seismic Network Monitoring Capability Algorithm. *Shanxi Earthq. Sci.* **2014**, 4, 1–3.
33. Wei, C.; Guo, D.; Chi, X.; Chen, L.; He, J. Monitoring Capability Analysis of Henan Regional Digital Seismic Network. *Seismomagn. Obs. Res*. **2017**, 38, 48–51.
34. Zhao, Z.; Zhang, R. Compilation of Zoning Travel Time Table of Seismic Waves in Sichuan. *Sichuan Earthq. Sci*. **1987**, 3, 29–35.
35. Wang, Y.; Tang, L.; Huang, C. One-Dimensional Crustal Velocity Model in Sichuan. *Sichuan Earthq. Sci.* **2019**, 3, 8–12.